Analysis of multiple time scales in a transistor amplifier

Douglas N. Armstead* and Thomas L. Carroll
US Naval Research Laboratory, Washington, DC 20375, USA
(Received 8 June 2004; revised manuscript received 10 September 2004; published 17 March 2005)

It was shown previously in an experiment that when high frequency signals (on the order of 1 MHz) were injected into this low frequency amplifier, the nonlinearities of the *pn* junctions caused period doubling, chaos, and very low frequency oscillations (on the order of 1 Hz). In this paper we present theory and simulations to explain the existence of the low frequency oscillations.

DOI: 10.1103/PhysRevE.71.036208 PACS number(s): 05.45.Ac, 84.30.−r

I. INTRODUCTION

In previous work [1] experiments showed that driving a simple one-transistor audio amplifier, Fig. 1, with a high frequency (approximately 1 MHz) signal could induce chaos, period doubling, and low frequency (on the order of 1 Hz) switching.

Chaos and period doubling in such a system might be expected based on studies of the diode resonator [2–11], in which a periodic signal is applied to a circuit consisting of an inductor, a resistor, and a diode. The inductor combined with the nonlinear capacitance of the diode form a nonlinear resonant system, which may exhibit period doubling or chaos. Similar low frequency oscillations were seen in a simple circuit using a diode [11], however, the authors made approximations that limited the applicability of their analysis to the driving regime that we consider.

In our previous experimental work, we were interested in what sort of nonlinear effects might be seen if a low frequency system containing *pn* junctions (such as our amplifier) was subjected to high frequency rf signals. The rf signals might be accidently produced by nearby communications systems, or they might be intentionally beamed at the circuit in an attempt to disrupt the functioning of the circuit. The inductances of the wires of the circuit combined with the capacitance of the *pn* junctions in the transistor formed the nonlinear resonant system, with a resonant frequency on the order of GHz.

The actual rf signals might have frequencies on the order of 1 GHz, but systems that can digitize signals fast enough to study GHz phenomena are still quite expensive, so we added an inductor to the input of the transistor amplifier in order to lower the resonant frequency of the inductor-*pn* junction combination.

II. EXPERIMENTAL DESCRIPTION

We consider a simple audio frequency transistor amplifier, Fig. 1. The transistor is a 2n929 bipolar transistor. The transistor has variable internal capacitance (Fig. 2) from a number of mechanisms (i.e., junction capacitance, diffusion capacitance) with a magnitude of order $C_0 \approx 10^{-11}$ F.

This capacitance gives the circuit a natural resonance near the frequency $f_0 = 1/\sqrt{4\pi^2 L C_0} \approx 1$ MHz (N.B. The inductor L was explicitly added to make the experiment easier to perform. There are inductances inherent in the wires and typical values give resonances on the order of GHz, which makes data collection difficult.) Driving the circuit with a signal with frequency f near f_0 causes the circuit to respond at the driving frequency f and also exhibits a low frequency switching on the order of 5–10 Hz. The experimentally determined switching frequency for a range of driving frequencies and driving amplitudes appear in Fig. 13.

III. THEORY

In order to simplify our analysis, we eliminate circuit elements which are not necessary for low frequency switching. Resistors R_1 and R_2 are present for biasing purposes and can be removed by biasing the input signal. The circuit is a voltage amplifier, not a current amplifier, so the resistor R_L can be removed and V_{cb} can be though of as the circuit output. Experiments and numerical simulations show that C_1 and C_2 do not affect the dynamics. C_1 and C_2 are present to isolate the amplifier from input and output dc levels.

Removing capacitors C_1 and C_2 reduces the dimensionality of the system without substantially changing the dynamics of the circuit. This somewhat simpler circuit (Fig. 3) exhibits similar behavior to the experimental circuit. At the audio frequencies the circuit is designed for, the inductor and the capacitances in the transistor are unimportant. At these low frequencies when the voltage across the base-emitter junction V_{be} is below a threshold value V_0 the transistor is

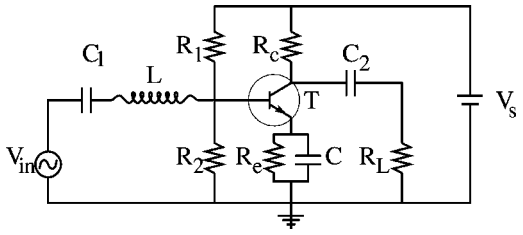

FIG. 1. A simple, stable, audio frequency transistor amplifier. $V_s = 15$ V, $R_1 = 40.42$ kΩ, $R_2 = 204.545$ kΩ, $R_c = 15$ kΩ, $R_e = 3.75$ kΩ, $R_L = 1$ MΩ, $C_1 = C_2 = 25$ μF, $C = 330$ μF, $L = 2200$ μH, and the transistor T is of type 2n929. The output of the circuit is across the load resistor R_L.

*Electronic address: armstead@anvil.nrl.navy.mil

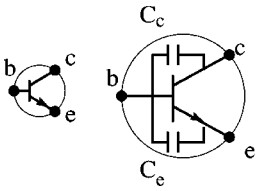

FIG. 2. The transistor has small variable internal capacitances C_c and C_e that are known to be frequency dependent.

nonconducting. Note that in general we define V_{ab} to be the voltage drop from point *a* to point *b*. For the transistor control voltage V_{be} above the threshold a small current will flow (at least for a bipolar junction transistor) from the base of the transistor (point *b*) to the emitter of the transistor (point *e*). This small current from *b* to *e* stimulates a much larger current from the collector (point *c*) out the emitter. The much larger collector-emitter current is proportional to $V_{be}-V_0$, at least for $V_{be}-V_0$ small. In this mode of operation the transistor acts as a voltage valve. For $V_{be}-V_0\approx 0$ very little current flows and most of the voltage drop across the amplification power source V_s occurs across the the collector-base junction (i.e., $V_{ac}\approx 0$ and $V_{cb}\approx V_s-V_{in0}$ where V_s is the amplifier power supply voltage and V_{in0} is the input signal biasing) whereas for large values of $V_{be}-V_0$ a large current flows and most of the current drop is across the resistor R_c (i.e., $V_{ac}\approx V_s-V_{in0}$ and $V_{cb}\approx 0$).

At the frequencies we consider in this paper all four reactive elements in the circuit in Fig. 3 are important: the inductor L, the capacitor C, and the two internal capacitances of the transistor C_c and C_e. As a result, the circuit can be described using four ordinary differential equations (ODEs):

$$\begin{aligned}
\frac{dI}{dt} &= \frac{1}{L}(V_{in}-V_{be}-V_{eg}),\\
\frac{dV_{cb}}{dt} &= \frac{1}{C_c}(V_{ac}/R_c - I_c),\\
\frac{dV_{be}}{dt} &= \frac{1}{C_e}(V_{ac}/R_c + I - I_e),\\
\frac{dV_{eg}}{dt} &= \frac{1}{C}(V_{ac}/R_c - I - V_{eg}/R_e),
\end{aligned} \tag{1}$$

where $V_{in}=V_{in0}+V_A\sin(2\pi ft)$, I is the current through the inductor, and I_c and I_e are the nonlinear currents which come from an Ebers-Moll description of the transistor,

$$I_c = I_0[-(e^{-qV_{cb}/kT}-1)+\alpha(e^{qV_{be}/kT}-1)],$$

$$I_e = I_0[(e^{qV_{be}/kT}-1)-\alpha(e^{-qV_{cb}/kT}-1)],$$

where $I_0=10^{-11}$, k is Boltzmann's constant, T is the temperature in K, and $\alpha=0.995$ is the fraction of current lost through the base of the transistor.

We now make a number of simplifying assumptions:

(i) The experimental effect was seen with different types of transistors, including both bipolar and field-effect transistors (FETs). From this we infer that the details of the nonlinearity of the current function are unimportant, so we approximate the exponential nonlinearity in the current function with a piecewise linear form (as was done for the diode resonator in Refs. [7,8]) linearized about the voltage V_0, at which the nonlinearity becomes important.

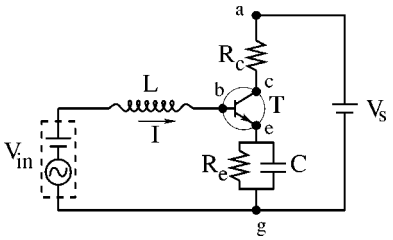

FIG. 3. A much simpler circuit that exhibits the same behavior as Fig. 1. For the numerical work done on this circuit we use the parameters $V_s=15$ V, $R_c=5$ kΩ, $R_e=10$ kΩ, $C_0=20$ μF, $C=3$ μF, $L=2000$ μH, $V_{in}=V_{in0}+V_A\sin(2\pi ft)$, $V_{in0}=2$ V.

(ii) Simulations show that the nonlinear capacitance is not necessary for the low frequency oscillations, therefore a constant capacitance is C_0 is used for the transistor capacitance.

(iii) The collector-base junction is never driven into a forward bias so the V_{cb} contributions to the nonlinear currents are small. The circuit will not be driven in such a way that the base-emitter junction will receive a large reverse bias.

(iv) The leakage of base current, while important for the proper functioning of a bipolar transistor, is not important for the FETs. In light of this we use $\alpha=1$.

(v) The large capacitance of C compared to both the transistor's internal capacitance (i.e., $C_0/C\ll 1$) and the inductance L [i.e., $L/(R_EC)\ll 1$] means that the dynamics of V_{eg} are much slower than those of the other variables. As a result, V_{eg} can be treated as a constant compared to the other variables, i.e.,

$$\frac{dV_{ac}}{dt} = \frac{d(V_s-V_{cb}-V_{be}-V_{eg})}{dt} \approx -\frac{dV_{cb}}{dt}-\frac{V_{be}}{dt}. \tag{2}$$

With these assumptions we rewrite the physical representation of the circuit Eqs. (1) in more natural coordinates:

$$\begin{aligned}
\frac{dx_1}{d\phi} &= \gamma[\sin(2\pi\phi)-x_3-y],\\
\frac{dx_2}{d\phi} &= -\delta[x_1+2x_2-2\kappa x_3 H(x_3)],\\
\frac{dx_3}{d\phi} &= \delta[x_1+x_2-\kappa x_3 H(x_3)],\\
\frac{dy}{d\phi} &= \epsilon[\lambda(x_1+x_2)-y-y_0],
\end{aligned} \tag{3}$$

where $x_1=R_cI/V_A$, $x_2=V_{ac}/V_A$, $x_3=(V_{be}-V_0)/V_A$, $y=V_{eg}/V_A-y_0$, $y_0=(V_{in0}-V_0)/V_A$, $\phi=ft$, $\gamma=R_c/fL$, f is the frequency of the input signal, $\delta=1/fR_cC_0$, $\epsilon=1/fR_eC$, $\lambda=R_e/R_c$, $\kappa=qR_cI_0/kT\exp(qV_0/kT)$, and $H(x)$ is the Heavyside step

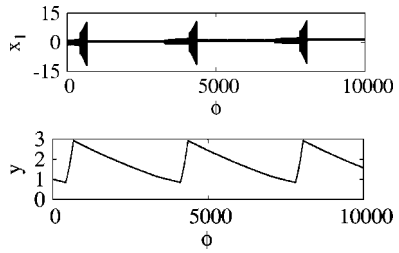

FIG. 4. Numerical integration of Eq. (3) over a number of slow switching cycles. x_1 is a slowly varying high frequency oscillation, whereas y varies only at the slower time scale.

function, which has a value of 0 for $x<0$ and 1 for $x>0$. For the relevant circuit parameters (see Fig. 3) all parameters that appear in Eqs. (3) are of order 1, except $\epsilon \sim O(10^{-3})$ and $\kappa \sim O(10^3)$.

Numerical integration of Eqs. (3) yields behavior that is substantially the same as is seen in the experiment. Figure 4 shows that one variable (y) varies on a much slower time scale than the others, which are periodic in the drive frequency. The fast variables x_1, x_2, and x_3 are bistable: for a given value of y, they occupy one of two different attractors. Figure 5 shows the two sets of possible wave forms for x_1, x_2, and x_3: the wave forms in Fig. 5(a) have larger amplitudes than the wave forms in Fig. 5(b). The wave forms gradually evolve as y slowly changes until the system suddenly switches from one wave form set to the other [e.g., from those depicted in Fig. 5(a) to those in Fig. 5(b)].

This switching between wave forms is captured in Fig. 6 which shows x_2, the normalized voltage across the resistor R_c, against y strobed once per drive cycle. Figure 6 shows the low frequency switching between the high amplitude state and the low amplitude state. In the high amplitude state (shown with large pluses) a large rectified current flows through R_c and into the transistor collector. This dc biased current flows through the transistor and charges capacitor C, increasing y until $y=y_{max}$ when the system switches into the low amplitude state (shown with small crosses). In the low

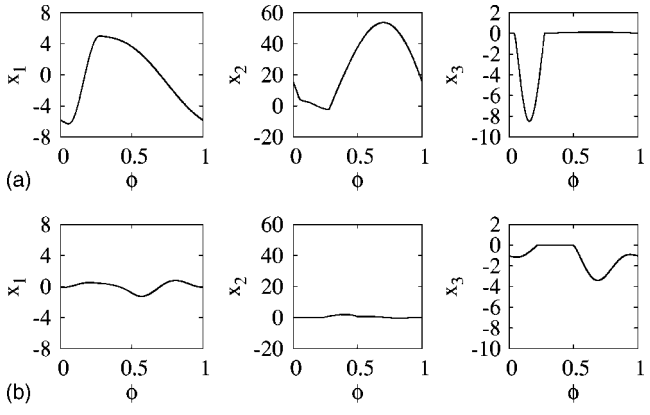

FIG. 5. Numerical integration of Eq. (3) over one period of the drive function. Set (a) is from the high amplitude state and shows the high amplitude wave forms of x_1, x_2, and x_3. Set (b) is from the low amplitude state and shows the low amplitude wave forms of x_1, x_2, and x_3. Both sets are for the same value of $y=1.15$.

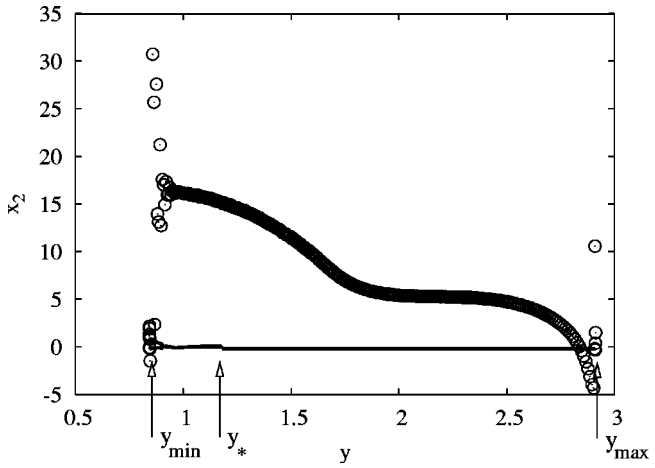

FIG. 6. Numerical integration of Eq. (3) over one slow switching cycle strobed once per drive cycle. The system evolves along the orbit in a clockwise sense. Initially in the low amplitude state, small +/narrow line, the system switches to the high amplitude state, large ⊙/wide line, at $y=y_{min}$ and switches from the high amplitude state to the low amplitude state at $y=y_{max}$. Upon re-entering the low amplitude state the transistor is strictly off from $y=y_{max}$ down to $y=y_*$.

amplitude state for $y_{max}>y>y_*$, x_3 is strictly less than zero. As a result the transistor does not conduct and there is no longer a rectified current flowing through R_c. Even after x_3 starts making excursions above $x_3=0$, as in the example shown in Fig. 5, the rectified current is much smaller than in the high amplitude state. With rectification effectively stopped throughout the low amplitude state, time average of x_1 and x_2 over one drive oscillation (dc level) approaches zero. As a result, charging stops and the capacitor C discharges through R_e, the resistor in parallel with C, so y drops. As y nears y_{min}, the lower end of its range, the system becomes unstable, causing the system to switch back into the high amplitude state. This instability causes the system to switch back into the high amplitude state in a number of ways, depending on the input signal frequency. The system may switch directly from the period one low amplitude state to the high amplitude state, it may first pass into a period doubling cascade and become chaotic before switching to the high amplitude state, or the system may even pass through a period doubling cascade and then through an inverse period doubling cascade before switching to the high amplitude state.

The low frequency switching is part of a hierarchy of time scales relevant to this system. At the fastest time scales (times of order $1/\kappa \ll 1$) there is the reaction of the system to the transistor turn on (i.e., the nonlinear currents I_c and I_e switch on). There is an intermediate time scale (times of order 1) associated with the driving frequency. At the slowest time scales (times of order $1/\epsilon \gg 1$) is the variation in the slow variable y, which is responsible for the slow switching observed in this system. This hierarchy of time scales makes singular perturbation theory (SPT) [12] an attractive approach.

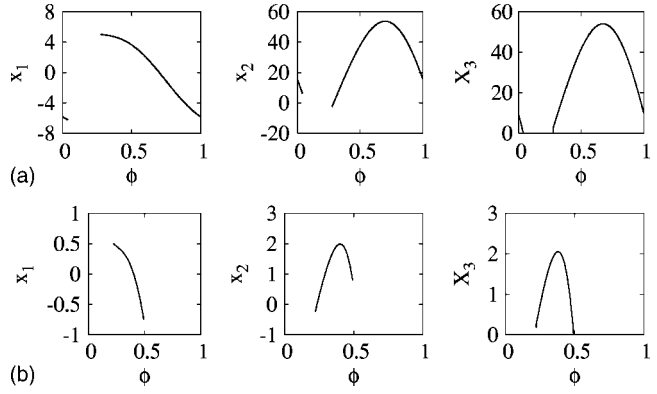

FIG. 7. While the transistor is conducting, the variables x_1, x_2, and $X_3=\kappa x_3$ are of the same order of magnitude. Numerical integration of Eq. (3) over one period of the drive function. Set (a) is from the high amplitude state and shows the high amplitude wave forms of x_1, x_2, and $X_3=\kappa x_3$ while $X_3 \geqslant 0$. Set (b) is from the low amplitude state and shows the low amplitude wave forms of x_1, x_2, and $X_3=\kappa x_3$ while $X_3 \geqslant 0$. Both sets are for the same value of $y=1.15$.

IV. SPT APPLIED TO TRANSISTOR EQUATIONS

In its simplest form SPT [12] allows one to make use of a small parameter ϵ to treat the fast and slow evolutions of a system separately. One does this by using two different parametrizations of time, t and $\tau=\epsilon t$. In the limit $\epsilon \to 0$ one obtains two distinct limiting behaviors, "fast equations" and "slow equations" for the t and τ parametrization, respectively.

The transistor equations have two extreme parameters (i.e., $\epsilon \ll 1$, and $\kappa \gg 1$) and so there are three time parametrizations we will consider: for the turn on time scale $\xi=\kappa\phi$, for the driving time scale ϕ, and for the slow switching time scale $\psi=\epsilon\phi$. From these three time parametrizations we will recover

(i) From the fast ξ time parametrization: the rapid change in x_3 when the transistor turns on.

(ii) From the intermediate ϕ time parametrization: the high and low amplitude states that constitute bi-stable limit cycle solutions for fixed y. Each limit cycle will contain two segments, one segment for which the transistor is conducting (On branch of the ϕ time parametrization manifold) and one segment for which the transistor is not conducting (Off branch of the ϕ time parametrization manifold). The two branches of the ϕ time parametrization manifold have different dimensionality due to different x_3 scaling.

(iii) From the slow ψ time parametrization: the equations that govern the evolution of the period-1 limit cycles along the two branches of the slow manifold as y changes.

Let us first consider the fastest time parametrization, ξ.

A. ξ time parametrization

When the transistor is conducting (i.e., $x_3 \geqslant 0$) the large parameter κ is present in Eqs. (3) and the ξ time parametrization of Eqs. (3) is relevant. In the ξ time parametrization when $x_3 \geqslant 0$ Eqs. (3) becomes

$$\begin{aligned}
\frac{dx_1}{d\xi} &= \frac{\gamma}{\kappa}[\sin(2\pi\phi) - x_3 - y], \\
\frac{dx_2}{d\xi} &= -\frac{\delta}{\kappa}(x_1 + 2x_2 - 2\kappa x_3), \\
\frac{dx_3}{d\xi} &= \frac{\delta}{\kappa}(x_1 + x_2 - \kappa x_3), \\
\frac{dy}{d\xi} &= \frac{\epsilon}{\kappa}[\lambda(x_1 + x_2) - y - y_0].
\end{aligned} \tag{4}$$

To apply SPT each of the variables must be of the same order of magnitude. In the conducting state (i.e., $x_3 > 0$) x_1, x_2, and x_3 are not of the same order of magnitude (see Fig. 5), whereas in the high amplitude state x_1 and x_2 vary by 10 and 50, respectively, x_3 varies by 0.003. However, x_1, x_2, and $X_3=\kappa x_3$ are of the same order of magnitude, Fig. 7 shows x_1, x_2, and X_3 only in the on state and each variable has a variation on the order of magnitude of tens in the high amplitude state and ones in the low amplitude state. Changing variables Eqs. (4) becomes

$$\begin{aligned}
\frac{dx_1}{d\xi} &= \frac{\gamma}{\kappa}[\sin(2\pi\phi) - X_3/\kappa - y], \\
\frac{dx_2}{d\xi} &= -\frac{\delta}{\kappa}(x_1 + 2x_2 - 2X_3), \\
\frac{dX_3}{d\xi} &= \delta(x_1 + x_2 - X_3), \\
\frac{dy}{d\xi} &= \frac{\epsilon}{\kappa}[\lambda(x_1 + x_2) - y - y_0].
\end{aligned} \tag{5}$$

In the limit $\kappa \to \infty$ Eqs. (5) reduces to

$$\begin{aligned}
\frac{dx_1}{d\xi} &= 0, \\
\frac{dx_2}{d\xi} &= 0, \\
\frac{dX_3}{d\xi} &= \delta[x_1 + x_2 - X_3], \\
\frac{dy}{d\xi} &= 0,
\end{aligned} \tag{6}$$

so that when the transistor begins conducting, only X_3 evolves and has the solution

$$X_3(\xi) = (x_1 + x_2)(1 - e^{-\delta(\xi-\xi_0)}), \tag{7}$$

where ξ_0 is the time at which the transistor turns on [i.e., $X_3(\xi_0)=0$].

The relaxation of X_3 from 0 to x_1+x_2 is very sudden when compared to the time scales of the ϕ parametrization. This can be seen by considering x_3 in terms of ϕ,

$$x_3(\phi) = \left(\frac{x_1 + x_2}{\kappa}\right)(1 - e^{-\kappa\delta(\phi-\phi_0)}). \tag{8}$$

Since $\kappa\delta \gg 1$, the time required for the transistor control variable x_3 to jump from the value $x_3=0$ to $x_3=(x_1+x_2)/\kappa$ is exceedingly small and in the ϕ parametrization we treat the jump in x_3 at the transistor turn on as a discontinuity.

B. ϕ time parametrization

In the ϕ parametrization there are two different scalings (X_3 and x_3) depending on whether the transistor is conducting [i.e., $H(X_3)=1$],

$$\begin{aligned}
\frac{dx_1}{d\phi} &= \gamma[\sin(2\pi\phi) - X_3/\kappa - y], \\
\frac{dx_2}{d\phi} &= -\,\delta(x_1 + 2x_2 - 2X_3), \\
\frac{1}{\kappa}\frac{dX_3}{d\phi} &= \delta(x_1 + x_2 - X_3), \\
\frac{dy}{d\phi} &= \epsilon[\lambda(x_1 + x_2) - y - y_0],
\end{aligned} \tag{9}$$

or not [i.e., $H(x_3)=0$],

$$\begin{aligned}
\frac{dx_1}{d\phi} &= \gamma[\sin(2\pi\phi) - x_3 - y], \\
\frac{dx_2}{d\phi} &= -\,\delta(x_1 + 2x_2), \\
\frac{dx_3}{d\phi} &= \delta(x_1 + x_2), \\
\frac{dy}{d\phi} &= \epsilon[\lambda(x_1 + x_2) - y - y_0].
\end{aligned} \tag{10}$$

These two different scalings give rise to different limiting behaviors. In the limit $\kappa\to\infty$ and $\epsilon\to 0$ we find

$$\begin{aligned}
\frac{dx_1}{d\phi} &= \gamma[\sin(2\pi\phi) - y], \\
\frac{dx_2}{d\phi} &= -\,\delta(x_1 + 2x_2 - 2X_3), \\
0 &= \delta(x_1 + x_2 - X_3), \\
\frac{dy}{d\phi} &= 0
\end{aligned} \tag{11}$$

and

$$\begin{aligned}
\frac{dx_1}{d\phi} &= \gamma[\sin(2\pi\phi) - x_3 - y], \\
\frac{dx_2}{d\phi} &= -\,\delta(x_1 + 2x_2), \\
\frac{dx_3}{d\phi} &= \delta(x_1 + x_2), \\
\frac{dy}{d\phi} &= 0
\end{aligned} \tag{12}$$

for Eqs. (11) and (12), respectively.

We therefore have two branches of Eqs. (3) for the ϕ time parametrization. The On branch [i.e., $H(X_3)=1$] solution is

$$\begin{aligned}
x_1 &= \gamma\left(-\frac{\cos(2\pi\phi)}{2\pi} - y\phi + A_1\right), \\
x_2 &= \delta\gamma\left(-\frac{\sin(2\pi\phi)}{4\pi^2} - \frac{y}{2}\phi^2 + A_1\phi + A_2\right), \\
X_3 &= x_1 + x_2, \\
y &= A_3
\end{aligned} \tag{13}$$

(where A_1, A_2, and A_3 are constants of integration), and the Off branch [i.e., $H(x_3)=0$] is

$$\begin{aligned}
\frac{dx_1}{d\phi} &= \gamma[\sin(2\pi\phi) - x_3 - y], \\
\frac{dx_2}{d\phi} &= -\,\delta(x_1 + 2x_2), \\
\frac{dx_3}{d\phi} &= \delta(x_1 + x_2), \\
\frac{dy}{d\phi} &= 0.
\end{aligned} \tag{14}$$

The Off branch (14) is linear and can be readily solved. The solution is composed of a transient piece coming from the autonomous equations and a particular solution which is

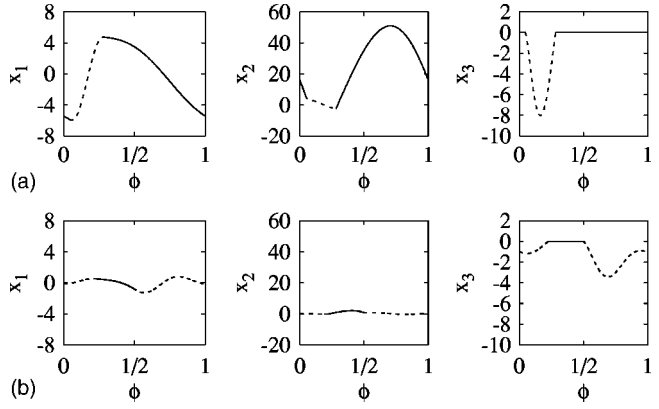

FIG. 8. Solutions for x_1, x_2, and x_3 in the (a) large amplitude state and (b) low amplitude state are found by piecing together an On state (solid line) with an Off state (dashed line) and demanding that the resulting wave form be periodic in the drive frequency. The agreement between these wave forms and the numerically integrated wave forms of Fig. 5 is exceptional.

nontransient. Both are important for the long time behavior of the system because of the repetitive switching back and forth between the On and Off branches.

We piece together the fragments of the period one oscillation from the On and Off branches of the manifold for the ϕ time parametrization to find constants of integration subject to the following conditions: that x_1 and x_2 are continuous at each junction, (i.e., both the On to Off and Off to On junctions) (as was done for the diode resonator in Refs. [7,8]) $x_3=0$ at each junction, and $X_3=0$ (i.e., x_3 in the On branch) at the junction from Off to On.

Finding period one solutions with one piece each from the On and Off branches is sufficiently complicated to require a numerical solution. To do this we use the first five conditions (i.e., $x_3=0$ at the Off to On junction and all conditions on x_1 and x_2) to determine the five constants of integration in terms of the two undetermined junction values of ϕ, ϕ_0, and ϕ_1. We then numerically solve for ϕ_0 and ϕ_1 subject to the conditions $x_3=0$ and $X_3=0$ at the On to Off junction. Within such a scheme finding values for ϕ_0 and ϕ_1 is tantamount to finding a potential period-1 solution. In searching for period-1 solutions with one piece from the On branch and one from the Off branch, we find a very limited number of solutions. The stable solutions correspond to the period-1 limit cycles of the large amplitude and low amplitude states. Examples for x_1, x_2, and x_3 in both states with $y=1.15$ are shown in Fig. 8. The agreement between these wave forms and the numerically integrated wave forms of Fig. 5 is excellent.

C. ψ time parametrization

In the previous subsection we found the stable period-1 limit cycles that are the typical solution for the ϕ time parametrization. (As previously noted, near the transition from the low amplitude state branch of the slow manifold the solution may, for some parameter values, go through a period doubling cascade to chaos. Period doubling is not a necessary condition for low frequency switching.) We now study the slow manifold that the system spends most of its time evolving along so that we might understand when the system will leave one branch of the slow manifold (the high amplitude state) and move to the other branch of the slow manifold (the low amplitude state), and when it will complete a low frequency switching cycle by returning to the high amplitude state.

Since x_1, x_2, and x_3 vary greatly over a period-1 oscillation it is convenient to consider the period one average of Eqs. (3). For a function $f(\phi)$ that has a period of 1, by definition $f(\phi+1)=f(\phi)$. As a result

$$\int_{\phi}^{\phi+1} \frac{df(\phi')}{d\phi'} d\phi' = f(\phi+1) - f(\phi) = 0.$$

Since x_1, x_2, and x_3 are each period 1, the equations for the period-1 average of Eqs. (3) are

$$\begin{aligned} 0 &= \gamma[-\langle x_3\rangle - \langle y\rangle], \\ 0 &= -\delta[\langle x_1\rangle + 2\langle x_2\rangle - 2\kappa\langle x_3 H(x_3)\rangle], \\ 0 &= \delta[\langle x_1\rangle + \langle x_2\rangle - \kappa\langle x_3 H(x_3)\rangle], \\ \frac{d\langle y\rangle}{d\psi} &= \lambda(\langle x_1\rangle + \langle x_2\rangle) - \langle y\rangle - y_0 \end{aligned} \tag{15}$$

where $\psi=\epsilon\phi$ and $\langle z\rangle=\int_{\phi}^{\phi+1} z d\phi/1$ is the average of z over one drive cycle. Solving for the averages yields

$$\begin{aligned} \langle x_1\rangle &= 0, \\ \langle x_2\rangle &= \kappa\langle x_3 H(x_3)\rangle, \\ \langle x_3\rangle &= -\langle y\rangle, \\ \frac{d\langle y\rangle}{d\psi} &= \lambda\kappa\langle x_3 H(x_3)\rangle - \langle y\rangle - y_0. \end{aligned} \tag{16}$$

The period-1 average equations determine the evolution of the system along the slow manifold. The average $\kappa\langle x_3 H(x_3)\rangle=\langle X_3 H(X_3)\rangle$ is readily calculable from our results in the ϕ time parametrization subsection.

When the current branch of the slow manifold consists of only period-1 oscillations we can say a bit about the switching point y_{min} for the low amplitude state or y_{max} for the high amplitude state. Numerical searches of the solution space for period-1 oscillations show that for y sufficiently close to the switching point there are two solutions [(a) and (b)] with values of ϕ_0 and ϕ_1 ($\phi_0^{(a)}$, $\phi_1^{(a)}$ and $\phi_0^{(b)}$, $\phi_1^{(b)}$, respectively) near each other. As y approaches the switching point the two solutions converge (i.e., $\phi_0^{(a)}-\phi_0^{(b)}\to 0$ and $\phi_1^{(a)}-\phi_1^{(b)}\to 0$). Beyond this value of y our numerical search fails to find any nearby solution.

If the circuit parameters are such that the system passes through a period doubling cascade before switching from the low amplitude state to the high amplitude state, then our period-1 analysis of the low amplitude state breaks down. The period doubling cascade to chaos is typically entered

TABLE I. A comparison of the range of (y_{min},y_{max}) from numerical simulation to the range found using the above analysis. Also the value of $\kappa\lambda\langle x_3 H(x_3)\rangle$ at three values of y where $y_{mid}=(y_{min}+y_{max})/2$. For reference y_0 ranges from 3 to 30.

Frequency f (kHz)	Simulation (y_{min},y_{max})	Analysis (y_{min},y_{max})	$\lambda\kappa\langle x_3 H(x_3)\rangle$ at $(y_{min},y_{mid},y_{max})$
150	(0.83, 2.52)	(0.96, 2.19)	(204, 282, 310)
200	(0.90, 2.72)	(0.98, 2.54)	(92.0, 122.6, 145.8)
250	(0.83, 2.91)	(0.96, 2.80)	(48.8, 72.2, 85.2)
300	(0.93, 3.11)	(0.93, 3.04)	(28.0, 42.4, 49.4)
	(0.52, 1.09)		
350	(1.23, 3.34)	(1.23, 3.30)	(19.7, 26.8, 29.4)
	(0.54, 1.14)		
400	(1.66, 3.60)	(1.67, 3.58)	(13.9, 16.9, 16.4)
	(0.55, 1.18)		
450	(2.33, 3.93)	(2.34, 3.93)	(9.4, 10.2, 9.4)
	(0.52, 1.21)		
500	(0.51, 1.22)	(−)	(−)
550	(0.48, 1.22)	(−)	(−)
600	(0.51, 1.22)	(−)	(−)
650	(0.53, 1.20)	(−)	(−)
700	(0.54, 1.17)	(−)	(−)
750	(0.54, 1.12)	(−)	(−)

when the period-1 solution for the low amplitude state is suddenly destroyed. This state is destroyed when a second local maximum in x_3 pushes up through the transistor turn on value. At this point our formal solution to the period-1 oscillation is no longer valid because the Off branch solution has a range of ϕ values for which $x_3>0$ which violates the definition of the Off branch.

V. RANGE AND SWITCHING FREQUENCY

We now estimate the frequency of the switching f_s as a function of frequency f and driving amplitude V_A.

First we determine y_{min} and y_{max} directly from the analysis; y_{min} is the value of y at which the low amplitude branch ceases to exist and y_{max} is the value of y at which the high amplitude branch ceases to exist. We also determine y_*, in the low amplitude state the transistor remains strictly off over the interval (y_*,y_{max}) and, as a result, the particular solution (as opposed to the autonomous solution) is the dominant. We therefore define y_* as the largest value of y at which the particular solution of x_3 is tangent to the line $x_3=0$. Since the parameters of Eqs. (13) and (14) depend on f but not V_A, the search for y_{min}, y_{max}, and y_* is independent of V_A and need only be done once for each frequency. The results of this search appear in Table I and will be discussed shortly.

Figure 9 shows the length of the interval (y_{min},y_{max}) found by numerical integration of Eqs. (3). Interval length is only displayed for parameter values for which the system switched periodically. There are two distinct bands of

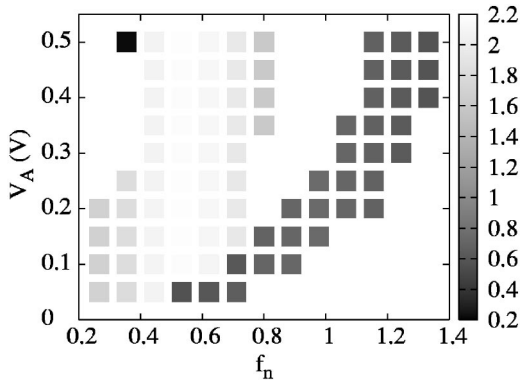

FIG. 9. The range over which y varies, $y_{max}-y_{min}$, as determined from numerical simulations, in the switching system with $f_n=f/f_0=f\sqrt{4\pi^2 L2C_0}$.

switching behavior in this graph: band 1 is present for $f_n<1$ with a large variation in y, and band 2 tends to occur at higher frequency and for which the variation in y is smaller. These two bands arise from qualitatively different behavior. In band 1 the low and high amplitude branches of the slow manifold are both period-1, whereas in band 2 the high amplitude branch is period-2. This puts a full discussion of band 2 out of the realm of the analysis in this paper.

There are frequencies for which both bands are present for the same frequency but different values of V_A. At these frequencies the high amplitude branch of band 1 is also the low amplitude branch of band 2.

Table I lists the range of (y_{min},y_{max}) from numerical simulation of Eqs. (3) as well as the range found using the above analysis. Although our analysis fails to detect band 2 the agreement between numerical simulations and our analysis is quite good for band 1. Our analysis provides an upper bound for y_{min} and a lower bound for y_{max}, the switch from low amplitude branch to high amplitude branch (and vice versa) will not happen before the low amplitude branch becomes unstable but the system may linger near before switching to the high amplitude branch. In practice the system does not linger long, and we note from Table I that as $f_n\to 1$ the values of y_{min} and y_{max} from the simulation approach the bound set by our analysis.

In addition to the range over which y varies we need to know how quickly y varies. Recall from Eqs. (16) that it is necessary to compute $\lambda\kappa\langle x_3 H(x_3)\rangle=\lambda\langle(x_1+x_2)H(x_3)\rangle$, which is proportional to the current that flows through the transistor and into the capacitor C while the transistor is on. Instead of computing $\lambda\kappa\langle x_3 H(x_3)\rangle$ at a dense set of points along the interval (y_{min},y_{max}), we calculate $\lambda\kappa\langle x_3 H(x_3)\rangle$ at a few points $[y_{min}$, $(y_{max}+y_{min})/2$, and y_{max} for the high amplitude state, and only at y_{min} for the low amplitude state because $\langle x_3 H(x_3)\rangle=0$ over the interval $(y_*,y_{max})]$ and linearly interpolate in between.

Our estimates of $\lambda\kappa\langle x_3 H(x_3)\rangle$, y_{min}, y_{max}, and y_* allow us to integrate the $\langle y\rangle$ equation of Eqs. (16) (i.e., the one drive cycle average equation for y) over one switching period. We break the integration up into the four regions of Fig. 10. The system evolves around the orbit in Fig. 10 a clockwise sense

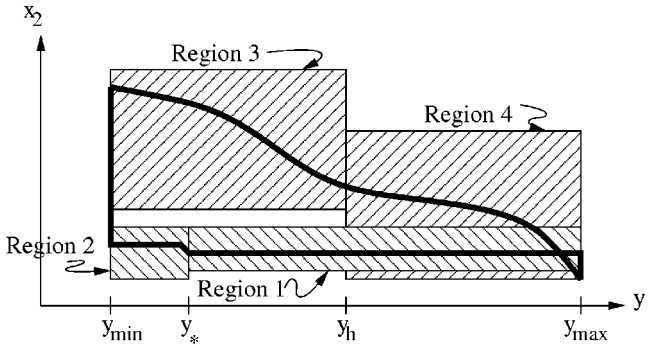

FIG. 10. The four regions over which the integration has been broken to find the switching frequency f_s. The system goes around the orbit in a clockwise rotation.

(i.e., it starts at y_{max} in region 1 and then at y_* passes into region 2, etc.). Integrating the $\langle y \rangle$ equation of Eqs. (16) and inverting yields the time the system spends in region i:

$$\Delta\phi_i = \frac{1}{\epsilon(\lambda m_i - 1)} \ln\left(\frac{y_{ei} + \tilde{y}_{0i}}{y_{si} + \tilde{y}_{0i}}\right), \tag{17}$$

where $\Delta\phi_i$ is the time spent in region i, y_{si} is the value of y at the start of the region, y_{ei} is the value of y at the end of the region, $\tilde{y}_{0i} = (\lambda b_i - y_0)/(\lambda m_i - 1)$, and the linearization of $\lambda\kappa\langle x_3 H(x_3)\rangle$ has parameters m_i and b_i such that $m_i y + b_i \approx \lambda\kappa\langle x_3 H(x_3)\rangle$ in region i. For example, in region 1 $y_{s1} = y_{max}$, $y_{e1} = y_*$, $m_1 = b_1 = 0$, and $\tilde{y}_{01} = -y_0$. Summing the time contribution from all four regions yields our estimate of the slow switching period T_s and the switching frequency $f_s = 1/T_s$. In Fig. 11 we present the normalized switching frequency, $F_s = \tau_{RC} f_s$ where $\tau_{RC} = R_e C$, for a range of fs and V_As.

Notice that for a fixed value of f, some values of V_A have an estimate for F_s and others there is none. For those that do not, either the value of $\kappa\lambda\langle x_3 H(x_3)\rangle$ at y_{min} on the high amplitude branch was so small that $\langle y \rangle$ would not grow (i.e., $\kappa\lambda \langle x_3 H(x_3)\rangle|_{\text{at } y=y_{min}} - y_{min} - y_0 < 0$), or the high amplitude branch became stable [i.e., $\kappa\lambda \langle x_3 H(x_3)\rangle|_{\text{at } y=y_{min}} - y_{min} - y_0 > 0$ but either $\kappa\lambda \langle x_3 H(x_3)\rangle|_{\text{at } y=y_h} - y_h - y_0 < 0$ or $\kappa\lambda \langle x_3 H(x_3)\rangle|_{\text{at } y=y_{max}} - y_{max} - y_0 < 0$]. Each of these estimates is for a band 1 f_s. Band 2 oscillations are possible in regions where band 1 oscillations are not because the period-2 high amplitude branch in band 2 has a large enough dc bias to charge C, even at lower values of V_A when the period-1 high amplitude branch cannot.

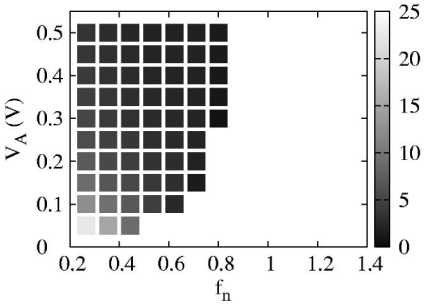

FIG. 11. The normalized switching frequency, $F_s = \tau_{RC} f_s = R_e C f_s$, as determined from the above analysis. The normalized driving frequency is $f_n = f/f_0 = f\sqrt{4\pi^2 L 2C_0}$. Only band 1 appears because our analysis does not apply to band 2.

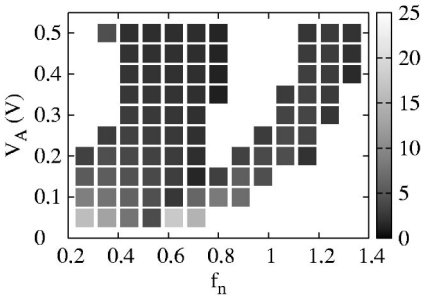

FIG. 12. The normalized switching frequency F_s as deduced from numerical simulations by the technique described in the text. The normalized driving frequency is $f_n = f/f_0 = f\sqrt{4\pi^2 L 2C_0}$.

We now wish to compare our results to those of numerical integration of the whole system. Towards this end we must calculate the switching frequency f_s from the numerical integration of Eqs. (1). From the time series we find the times of each maxima in the variable y and record the average interval between maxima, $\langle T_{int}\rangle$, when the standard deviation in the intervals is less than $\langle T_{int}\rangle/4$. This is to exclude parameter values for which the behavior is nonperiodic in nature. This excludes some data for low frequencies and larger driving amplitudes ($f_n \leqslant 0.4, V_A > 0.25$) that is closer to bursting in behavior. The record of this for a range of fs around the natural frequency of the system, $f_0 = 1/\sqrt{4\pi^2 L 2C_0}$, and a range of driving amplitudes V_As appears in Fig. 12. (The natural frequency depends on $2C_0$ instead of C_0 because the internal capacitors are parallel, and so their capacitances add.)

Within band 1 the agreement is quite good for higher driving frequencies. At lower driving frequencies the analysis suggests that there is switching behavior where the numerical simulation does not. If one consults Table I, one can see that as f decreases the $\lambda\kappa\langle x_3 H(x_3)\rangle$ becomes large. The SPT analysis is predicated on assumption that $d\langle y\rangle/d\phi$ is much less than $dx_j/d\phi$ where $j = 1$, 2, and 3, which may not be the case if $\lambda\kappa\langle x_3 H(x_3)\rangle$ is becoming large.

By considering the normalized switching frequency F_s instead of f_s we are able to compare our analysis and numerical integration with the results of the experimental work in [1] which are reproduced in Fig. 13. We chose a smaller

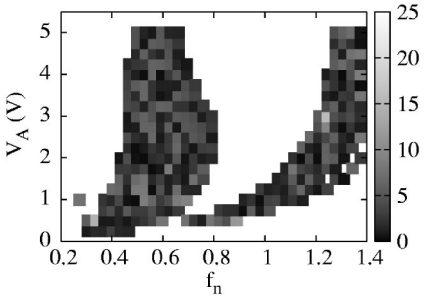

FIG. 13. The normalized switching frequency F_s from the experiment in Ref. [1] where $f_n = f/f_0$ and $f_0 \approx 693$ kHz.

value of τ_{RC} (recall that $\tau_{RC}=R_eC$) for the numerical integration so that the integration could be done in a reasonable amount of time. For the experimental circuit $\tau_{RC}\approx 1.24$, for the numerical work the $\tau_{RC}=0.03$, and for the analytical work no assumption was necessary [from Eq. (17) f_s is proportional to $\epsilon=1/fR_eC$ and F_s is proportional to $\epsilon\tau_{RC}=1/f$].

There are several aspects of the experimental results from the circuit in Fig. 1 that are accounted for in the numerical integration and analysis of the simpler circuit in Fig. 3. The experimental results in Fig. 13 show two bands, one on either side of $f_n=1$. This is the same basic structure found in the numerical simulation. With regard to the analysis we note that band 1 of the analysis extends over to and no further than $f_n=0.8$, as is also the case for band 1 of the experimental results in Fig. 13. With regard to the switching frequencies, note that the majority of the values for F_s from our analysis and numerical integration fall within the same range of values as those found in the experiment.

VI. CONCLUSION

We have shown that the low-frequency switching in a class C amplifier, due to a modest amplitude signal at a frequency higher than the circuit was designed to operate at, can be understood using a singular perturbation analysis. In particular, by analyzing the high frequency (input signal frequency) response of the system we have been able to estimate the frequency of the slow behavior of the system. We also are able to predict one band of driving frequencies and amplitudes over which the slow behavior occurs. We expect that the techniques described in this paper could be extended to find the second observed band of driving frequencies and amplitudes over which the slow behavior occurs.

[1] T. L. Carroll, Phys. Rev. E **67**, 046208 (2003).
[2] T. L. Carroll and L. M. Pecora, Phys. Rev. E **66**, 046219 (2002).
[3] E. R. Hunt and R. W. Rollins, Phys. Rev. A **29**, 1000 (1984).
[4] C. M. Kim, C. H. Cho, C. S. Lee, J. H. Yim, J. Kim, and Y. Kim, Phys. Rev. A **38**, 1645 (1988).
[5] P. S. Linsay, Phys. Rev. Lett. **47**, 1349 (1981).
[6] Z. Su, R. W. Rollins, and E. R. Hunt, Phys. Rev. A **40**, 2698 (1989).
[7] N. Takeuchi, T. Nagai, and T. Matsumoto, Electron. Commun. Jpn., Part 2: Electron. **84**, 91 (2001).
[8] S. Tanaka, S. I. Higuchi, and T. Matsumoto, Phys. Rev. E **54**, 6014 (1996).
[9] J. Testa, J. Perez, and C. Jeffries, Phys. Rev. Lett. **48**, 714 (1982).
[10] R. MarizdeMoraes and S. M. Anlage, Phys. Rev. E **68**, 026201 (2003).
[11] V. A. Rylov and V. G. Elenskiy, Radio Eng. Electron. Phys. **10**, 1850 (1965).
[12] An excellent discussion of SPT in general and the subtleties of the van der Pol oscillator can be found in R. E. O'Malley, *Singular Perturbation Methods for Ordinary Differential Equations* (Springer-Verlag, New York, 1991).